

Photoionization of Galactic Halo Gas by Old Supernova Remnants

Jonathan D. Slavin¹

Department of Astronomy, University of California, Berkeley, CA 94720

Christopher F. McKee

Departments of Physics and Astronomy, University of California, Berkeley, CA 94720

and

David J. Hollenbach

NASA/Ames Research Center, MS 245-3, Moffett Field, CA 94035

ABSTRACT

We present new calculations on the contribution from cooling hot gas to the photoionization of warm ionized gas in the Galaxy. We show that hot gas in cooling supernova remnants (SNRs) is an important source of photoionization, particularly for gas in the halo. We find that in many regions at high latitude this source is adequate to account for the observed ionization so there is no need to find ways to transport stellar photons from the disk. The flux from cooling SNRs sets a floor on the ionization along any line of sight. Our model flux is also shown to be consistent with the diffuse soft X-ray background and with soft X-ray observations of external galaxies.

We consider the ionization of the clouds observed towards the halo star HD 93521, for which there are no O stars close to the line of sight. Along this line of sight, two groups of clouds (densities $\sim 0.3\text{--}1\text{ cm}^{-3}$ and temperatures $\sim 7000\text{ K}$) are observed at $\sim 0\text{ km s}^{-1}$ (“slow”) and $\sim -50\text{ km s}^{-1}$ (“fast”). We show that the observed ionization can be explained successfully by our model EUV/soft X-ray flux from cooling hot gas. In particular, we can match the $\text{H}\alpha$ intensity, the S^{++}/S^+ ratio, and the C^{++} column. Our models show that it is possible to account for the observed ionization without invoking exotic ionization mechanisms such as decaying neutrinos (Sciama 1990). Our value for X-ray opacity along this line of sight is somewhat larger than the average for the halo found by Arabadjis & Bregman (1999), but we do not regard the difference as significant. From observations of the ratios of columns of C^{++} and either S^+ or H^0 , we are able to estimate the thermal pressure in the clouds. The slow clouds require high

¹Postal address: NASA/Ames Research Center, MS 245-3, Moffett Field, CA 94035

($\sim 10^4 \text{ cm}^{-3} \text{ K}$) thermal pressures to match the $N_{\text{C}^{++}}/N_{\text{S}^+}$ ratio. Additional heating sources are required for the slow clouds to maintain their $\sim 7000 \text{ K}$ temperatures at these pressures, as found by Reynolds, Haffner & Tufte (1999).

Subject headings: ISM: general — supernova remnants — ISM: clouds — Galaxy: halo
— X-rays: ISM

1. Introduction

The nature of diffuse warm ionized gas (or warm ionized medium, WIM) in the interstellar medium has been puzzling since its discovery. In a series of articles, Reynolds (1984, 1985a,b, 1988, 1989a,b, and Reynolds & Tufte 1995) has pointed out several unusual properties of this gas including: high [S II] $\lambda 6716/\text{H}\alpha$ ratios; low [O I] $\lambda 6300/\text{H}\alpha$, [O III] $\lambda 5007/\text{H}\alpha$ and He I $\lambda 5876/\text{H}\alpha$ ratios; high scale height; and large power requirement for its ionization.

Among the characteristics of the WIM that are the most difficult to make sense of are its power requirement, its large scale height and its relative smoothness. The power required to maintain the ionization has been estimated by Reynolds (1984) to be $9 \times 10^{-5} \text{ ergs s}^{-1} \text{ cm}^{-2}$, putting severe constraints on the source of ionizing photons. Only OB stars and supernovae appear to fulfill this power requirement. Citing the high efficiency required for conversion of explosion energy into photoionization, Reynolds (1984) favored early type stars as the primary source for maintaining the WIM. There are two principal difficulties with this source, however. First, several lines of sight in the plane apparently do not pass sufficiently close to any O or B stars (Reynolds 1990). Equivalently, the relative smoothness of the $\text{H}\alpha$ background appears inconsistent with the very clumpy distribution of early type stars. Second, the large scale height observed for the emission, $\sim 1 \text{ kpc}$, is much higher than the stellar scale height. This problem has been addressed by Miller & Cox (1993) and by Dove & Shull (1994) by modeling the escape of Lyman continuum photons from the disk, particularly from OB associations. For some cases, however, even the existence of large “HII chimneys” cannot explain the ionization at high latitudes. A prime example of this is the line of sight towards HD 93521 that we discuss in detail below.

Cooling hot gas avoids some of these difficulties. First, although supernovae should have a scale height essentially identical to OB stars, hot gas is buoyant in the galactic gravitational field and rises to much larger scale heights. This is directly observed in the large scale heights of the highly ionized species C^{+3} , N^{+4} and Si^{+3} (Savage, Sembach & Lu 1997, and references therein). Second, hot gas by its very nature is a more smoothly distributed source of ionizing radiation than stars. While the effect of a single star or star cluster drops off with the square of the distance, the flux from hot gas, even distributed non-uniformly in regions of high emissivity, depends on the line of sight emission measure and thus tends to be much smoother. Nevertheless, the high efficiency required for conversion of SN energy into photoionizations remains. We do not argue in this paper that old supernova remnants are the sole or even primary source of the ionization responsible for

the entire diffuse galactic H α background. Rather we show that cooling hot gas sets a floor on the ionization level for diffuse gas in the ISM in general and the galactic halo in particular. Moreover, for at least the line of sight towards HD 93521 and most probably for many high galactic latitude sight lines, cooling hot gas *is* the dominant source of the ionization. Thus we find that in many cases there is no need to devise a means of transporting photons from early type stars in the disk to the galactic halo.

The ionizing flux produced by cooling hot gas cannot be measured directly because the photons responsible for most of the ionization lie in the 13.6 – 50 eV range, a part of the EUV for which the diffuse background has not yet been definitively detected (see Vallergera & Slavin 1998). We are therefore left to theoretical modeling to estimate the ionizing flux. Our procedure, detailed below, is to calculate a space and time averaged emissivity due to supernova remnants expanding in the ISM. The mean emissivity (along with an estimate of the fraction of ionizing photons that escape from the disk) gives us a prediction for the emission measure generated by photoionization due to hot gas emission. Using the emissivity and a simple model for the mean opacity in a cloudy medium interspersed with hot gas, we derive the mean intensity incident on a cloud face. [It should be noted that we use the term “cloud” to refer to any cold or warm ($T \lesssim 10^4$ K) region of gas that is embedded in much lower density ($n \sim 5 \times 10^{-3}$ cm $^{-3}$), hot ionized medium (HIM).] We are then able to calculate such observables as the C $^{+*}$ (C $^+$ in the excited fine structure level), S $^+$, and S $^{++}$ column densities per cloud as well as a typical value for the galactic soft X-ray background and the X-ray surface brightness of the Galaxy as viewed from the outside. As we show below, our model is remarkably successful in explaining a variety of observations. Thus, while our model is clearly too simple to explain all the detailed observations of the soft X-ray background and ionization in the halo, its success provides evidence that cooling hot gas is an important source of ionization for the WIM.

In §2 below we describe current evidence on emission from old SNRs and give details about our model calculations of that emission. In §3 we use our model to predict the emission measure and H α intensity generated by ionization due to hot gas emission and compare with observations. In §4 we look at other ionization predictions from the model and compare with observations towards the line of sight towards HD 93521. We discuss how observations of S II, S III, and C II* absorption lines constrain the morphology of the clouds and their thermal pressure, whereas [N II], [S II] and [O I] emission lines constrain the temperature. In §5 we describe how the ionization of helium in our model affects the X-ray opacity of the halo. In §6 we discuss the uncertainties in the model spectrum, the need for additional heating in the slow clouds, and the decaying neutrino model for the ionization proposed by Sciama (1990). Finally, we summarize our conclusions in §7.

2. The Soft X-ray Background from Old Supernova Remnants

2.1. Observations of the Local Background

The direct evidence for soft X-ray emission from hot gas comes primarily from proportional counter observations of the diffuse background by the Wisconsin group (e.g., McCammon et al. 1983) and by ROSAT (e.g., Snowden et al. 1997). The most important of these for the issue of ionization are the lower energy bands: the B and C bands (~ 150 and 250 eV) of the Wisconsin instruments and the R1 and R2 bands (~ 200 and 250 eV) defined for ROSAT. The all-sky maps produced by both sets of observations are essentially consistent with each other when allowances are made for the difference in filters, sensitivity and angular resolution (Snowden et al. 1995).

In the broadest terms, the observations show the whole sky to be glowing with soft X-ray emission with a general trend of greater brightness towards the poles. While there has been much discussion of the proper interpretation of the results (e.g., Cox 1998; McKee 1998), there is now a general consensus that most of the observed emission comes from a cavity in the neutral hydrogen that surrounds the Sun and is filled with hot ($T \approx 10^6$ K), very low density gas. At high latitude the $1/4$ keV (C band) background also has substantial contributions from more distant emission, in some directions dominating the local component. In the galactic plane this seems not to be the case, though the presence of low column density clouds, seen by optical and EUV absorption, has yet to be fully taken into account in the modeling of the observed flux (see Slavin 1998).

2.2. Models for the Soft X-ray Background

Several studies have been carried out to explain the origins of the soft X-ray emission. McKee & Ostriker (1977) put forward a comprehensive model for the diffuse ISM in which supernova remnants sweep the warm and cold gas into shells and isolated clouds, leaving most of the medium filled with hot gas. The observed local emission is seen as being somewhat greater than in the typical ISM due to our being in an old supernova remnant (their estimate corresponds to an age of about 3×10^5 yr). Cox & collaborators (Cox & Anderson 1982; Edgar 1986; Edgar & Cox 1993; Smith & Cox 1998) have explored a number of models aimed specifically at explaining the SXRb as the result of the Sun's position inside a supernova remnant (possibly due to several explosions). Our model that we present below is not aimed specifically at explaining the observed SXRb and is, in this sense, more like the McKee & Ostriker model. We do not attempt, however, to model the medium as a whole and our model of the emissivity does not rest on any particular model for the morphology of the ISM. On the other hand, our model for the flux incident on clouds does require assumptions about the distribution of opacity in the medium and we use this fact below to draw conclusions on typical cloud (i.e., WNM and WIM) sizes. In addition, the data for the line of sight towards HD 93521 gives us information on the typical pressures in clouds that we can use to set limits to the filling factor of warm clouds in this direction. We find, in accordance with Reynolds

(1991) and Spitzer & Fitzpatrick (1993), that the warm clouds have a fairly small filling factor, $\lesssim 10\%$ (see §4.3 below).

A model for the mean emission from a population of evolving SNRs has previously been calculated by Cox & McCammon (1986) for the purpose of constraining the properties of SNRs in the galaxy M101. They carried out analytical calculations of the distribution over temperature of the surface averaged emission measure. A set of numerical calculations similar to the ones we present here was performed by Miller (1994) again with observations of external galaxies in mind. The aim of our calculations is somewhat different, being focussed on the ionizing properties of the x-ray/EUV emission. At the time of publication of Cox & McCammon (1986), only upper limits to the soft X-ray emission were available. With the advent of *ROSAT*, the X-ray emission has been detected for M101 and a number of other galaxies. As we discuss below, the fraction of soft X-ray emission that escapes the galaxy provides one of the tests of our model. In addition, we examine in more detail the spectrum produced by the cooling, supernova-shocked gas and its effect on the ionization structure of the WIM and the WNM.

2.3. The Hot Gas Emission Model

The primary purpose of this paper is to explore the effects of photoionization by cooling hot gas in the galaxy. As a consequence, we have focussed on the calculation of the emission and have made very simple assumptions regarding the ISM. To calculate the mean emissivity, we assume independent evolution of SNRs expanding in a uniform density medium. The mean emissivity of the hot gas is then

$$\langle \epsilon_\nu \rangle = S \int dt \int \epsilon_\nu dV \quad (1)$$

where S is the supernova rate per unit volume, ϵ_ν is the emissivity per unit frequency in the remnant as a function of position and time within the remnant. The integration is carried out over the volume of the remnant and time evolution of the remnant. We shall generally work with quantities measured per unit area of the disk, so we define $S_A \equiv \int S dz$ as the supernova rate per unit area and $\langle \epsilon_{\nu A} \rangle \equiv \int \langle \epsilon_\nu \rangle dz$ as the mean emissivity per unit area. Normalizing to the explosion energy, E_{SN} we define:

$$\phi_\nu \equiv \frac{\langle \epsilon_\nu \rangle}{S E_{\text{SN}}} = \frac{\langle \epsilon_{\nu A} \rangle}{S_A E_{\text{SN}}}. \quad (2)$$

Thus ϕ_ν is the fraction of the supernova power radiated per unit frequency interval. Equation (2) shows that the total supernova power, or equivalently, the supernova power per unit disk area, is separable from the calculation of the mean spectrum that determines the emission characteristics of the SNRs. This formulation brings out the fact that it is this distribution in frequency that is critical in determining the photoionizing properties of the cooling hot gas in SNRs.

To carry out the calculations of ϕ_ν we perform high resolution numerical calculations using a 1-D (spherically symmetric) hydrodynamics code. This code, written by us, borrows from the VH-

1 code (see <http://wonka.physics.ncsu.edu/pub/VH-1/index.html>) and uses the same piecewise parabolic method (PPM) with a Lagrangian step followed by a remap onto the fixed grid. We include the non-equilibrium ionization of the gas and radiative cooling appropriate to the ionization. For these calculations the ionization, recombination and radiative cooling rates have been generated using the Raymond & Smith (1977, plus updates) codes. Care has been taken to assure that the remapping step conserves the mass in each ion stage. We have carried out resolution studies and have found that the results converged at high resolution. The spectra used in the results that follow are for our highest resolution (0.07 pc for the $n_a = 0.1 \text{ cm}^{-3}$ case, where n_a is the average ambient preshock hydrogen nucleus density of the medium into which supernovae expand). The evolution of a remnant has been followed until nearly all the energy has been radiated and a small fraction of the explosion energy remains in thermal energy. The spectrum is then generated using the temperature, density and ionization profiles as a function of remnant age. We have done some runs in which thermal conduction was included (using an operator splitting technique) with no inhibition of conduction other than the limitation imposed by saturation (Cowie & McKee 1977). We have found the differences in the resulting spectra to be relatively small and therefore do not present results for these cases in this paper. We have done runs for a variety of ambient density cases, $n_a = 0.04, 0.1, 0.3$ and 1.0 cm^{-3} . We assume an explosion energy of 10^{51} ergs in all cases. We do not include any magnetic field effects; this assumption is discussed below.

Having generated ϕ_ν (and thus the mean emissivity, $\langle \epsilon_\nu \rangle$, assuming SE_{SN} is known) we then need a model for the opacity of the medium in order to calculate the mean intensity, J_ν . The true opacity of the ISM to ionizing photons is clearly extremely complicated. It depends on the distribution of neutral hydrogen column density on scales ranging from 10^{18} cm^{-2} to 10^{20} cm^{-2} , including the correlations among clouds and local large scale structures. To create a realistic model for the opacity of the ISM is thus well beyond the scope of this paper. Nevertheless, any given cloud that is to be subject to the ionizing field generated by hot gas will receive radiation from sight lines that will pass through a range of cloud columns present in the medium. For this reason we adopt a model for the opacity that is as simple as possible while still allowing for an interspersion of emitting and absorbing material, as must be the case in the ISM.

Our approach is to assume a uniform medium in the sense that the clouds, assumed to be of some typical optical depth, $\tau_{c\nu}$, are distributed randomly in the hot gas. The optical depth due to these clouds at frequency ν is

$$\tau_\nu = \mathcal{N}_{\text{los}} (1 - e^{-\tau_{c\nu}}) \quad (3)$$

(Bowyer & Field 1969, see the Appendix), where \mathcal{N}_{los} is the expected number of clouds along the line of sight. The average value of the mean intensity in the disk and halo is

$$\bar{J}_\nu = \frac{1}{\tau_{0\nu}} \int_0^{\tau_{0\nu}} d\tau_\nu \frac{1}{4\pi} \int I_\nu d\Omega, \quad (4)$$

$$= \frac{\langle \epsilon_\nu A \rangle}{4\pi \tau_{0\nu}} (1 - \eta_\nu) \quad (5)$$

where $\tau_{0\nu}$ is the optical depth through the full disk and halo,

$$\eta_\nu = \frac{1}{\tau_{0\nu}} \left[\frac{1}{2} + E_3(\tau_{0\nu}) \right], \quad (6)$$

is the mean escape probability, and $E_3(\tau_{0\nu})$ is an exponential integral. As shown in the Appendix, this value of the mean intensity is approximately equal to the expected value of the mean intensity in the intercloud medium, provided it has a substantial filling factor.

Thus our model for the mean intensity incident on a cloud depends on five parameters: the cloud optical depth $\tau_{c\nu}$, the disk optical depth, $\tau_{0\nu}$, the SN explosion energy, E_{SN} , the supernova rate per unit area S_A , and ϕ_ν . The optical depths are related to the column densities by $\tau_{c\nu} = N_{\text{H}^0_c} \sigma_\nu$ and $\tau_{0\nu} = N_{\text{H}^0_\perp} / N_{\text{H}^0_c} [1 - \exp(-N_{\text{H}^0_c} \sigma_\nu)]$ (eq A22), where $N_{\text{H}^0_c}$ is the HI column through the standard cloud and $N_{\text{H}^0_\perp}$ is the total HI column of the disk and the halo perpendicular to the disk plane. The values for the column densities are discussed in §3 below. For S_A we use the results from McKee & Williams (1997), $S_A = 3.8 \times 10^{-5} \text{ kpc}^{-2} \text{ yr}^{-1}$ at the Solar Circle. However, for the line of sight toward HD 93521 we find it necessary to effectively reduce this number slightly in order to match the observed H α intensity. In general, E_{SN} and ϕ_ν are not independent, since the explosion energy will affect the evolution (temperature, ionization, etc.) of the remnant which in turn determines ϕ_ν . Nevertheless, the separation of the two quantities emphasizes the fact that ϕ_ν is the efficiency with which the available energy is radiated over frequency. Thus our formulation could be extended to other potential sources of ionizing radiation such as the conduction fronts surrounding evaporating clouds (McKee & Cowie 1977) or the interfaces in turbulent mixing layers (Slavin, Shull & Begelman 1993).

2.4. The Model X-ray/EUV Spectrum

Figure 1 shows our model X-ray/EUV spectrum compared with a collisional ionization equilibrium (CIE), $T = 10^6 \text{ K}$, unabsorbed spectrum. The latter is scaled so as to match the all-sky average B band count rate observed by the Wisconsin group (McCammon et al. 1983). Of particular note are the greater fluxes at low energies ($h\nu \sim 13.6 - 30 \text{ eV}$) in the cooling model as opposed to the CIE spectrum. As can be seen from the spectrum, these photons dominate the higher energy photons in producing ionization in interstellar clouds.

A great deal of effort has gone into modeling the observed diffuse soft X-ray background (SXRb) (e.g. Cox & Anderson 1982; Jakobsen & Kahn 1986; Snowden et al. 1998; Smith & Cox 1998). Our model has not been created with the aim of matching the SXRb observations. In particular, we do not attempt to match the plane to pole variation in intensity or the variation of the observed X-ray band count rate ratios with $N(\text{H I})$. These characteristics of the data apparently demand the existence of an irregularly shaped Local Bubble and as such are inconsistent with any simple global model. On the contrary, we have calculated a time and space averaged emission spectrum that should approximate the observed spectrum at high galactic latitudes, where the

lower H I density allows us to see farther along a line of sight and where there is clear evidence that the observed flux has substantial contributions from distant emission (Garmire et al. 1992).

For comparison of our model results to the data, we need to specify all the model parameters as described above. Of particular importance is $N_{\text{H}^0\perp}$, as it effectively determines the mean free path for the soft X-ray photons. The average disk column density at the solar circle is $6.2 \times 10^{20} \text{ cm}^{-2}$ (Dickey & Lockman 1990). However, the Local Bubble apparently has carved out a hole in the H I distribution, resulting in a substantially lower value of $N_{\text{H}^0\perp}$ locally. We use a value of $3.2 \times 10^{20} \text{ cm}^{-2}$ (Kulkarni & Fich 1985) for our comparisons at high latitude. For the typical cloud column density, we adopt $N_{\text{H}^0c} = 1.46 \times 10^{19} \text{ cm}^{-2}$, the mean value observed for clouds along the line of sight towards HD 93521. We use our standard spectrum ($n_a = 0.1 \text{ cm}^{-3}$, no conduction, and $E_{\text{SN}} = 10^{51} \text{ ergs}$) to determine ϕ_ν . In order to match the observed H α intensity toward HD 93521, we find it necessary to reduce S_A by a factor 0.68 (§3). In other words, the average supernova rate S_A at the Solar Circle creates enough cooling hot gas to produce somewhat more hydrogen ionization than is observed toward the particular line of sight to HD 93521; this clearly demonstrates that the ionizing power of supernova remnants is significant at high latitude. A slight reduction in S_A along this line of sight, or of the radiation field along this line of sight, is quite reasonable in view of the observed variations in the soft X-ray background (e.g. Snowden et al. 1997).

The most important comparison we can make with the data is a spatially averaged measurement at low energy. For this purpose, the Wisconsin B and C band data are the best choice. From the publicly available maps we find that for $|b| > 45^\circ$ the average count rates for the B and C bands are 63 and 184 counts s^{-1} , respectively. For the line of sight towards HD 93521, the count rates are 84 and 210 counts s^{-1} . There is a fair amount of scatter, with the B band rate ranging from 18 to 134 and the C band rate from 62 to 302. The C/B ratio shows somewhat less scatter, ranging from 1.7 to 8.2. For the parameter choices detailed above we find a B band rate of 70 and a C band rate of 202 counts s^{-1} . Given that we have made no attempt to vary the parameters of our model to fit the SXR data, we find this agreement remarkable.

2.5. Soft X-ray Emission from External Galaxies

Another test of our model is to compare it with the soft X-ray emission from external galaxies. This comparison has the advantage that local variations are averaged out, but the disadvantage that various conditions affecting the strength and spectrum of the emission (e.g. n_a , S_A) could be significantly different in other galaxies. We estimate the X-ray luminosity of the Galaxy using the average conditions at the solar circle; thus, we use $N_{\text{H}^0\perp} = 6.2 \times 10^{20} \text{ cm}^{-2}$ for the disk thickness, $S_A = 3.8 \times 10^{-5} \text{ kpc}^{-2} \text{ yr}^{-1}$ for the SN rate per unit area, and 530 kpc^2 for the effective area of the disk (McKee & Williams 1997). Using equations (5) and (6), we find that the total luminosity in ionizing photons that escape from the disk in this case is $1.1 \times 10^{40} \text{ ergs s}^{-1}$, while the luminosity in X-ray photons ($E > 100 \text{ eV}$) is $2.2 \times 10^{39} \text{ ergs s}^{-1}$. Note that our estimate for the ionizing

luminosity is very sensitive to our assumption that the emission and absorption are uniformly mixed; our estimate for the X-ray luminosity also depends on this assumption, although to a lesser extent (see the Appendix).

Observations of diffuse soft X-ray emission in external galaxies are quite difficult. Proper accounting for point sources, backgrounds and galactic absorption are required (Cui, Sanders & McCammon 1996, hereafter CSM). The intensity or emission measure estimates that result are not tightly constrained. CSM observed five galaxies (NGC 3184, NGC 4736, M101, NGC 4395 and NGC 5055) in the R12 or R12L bands of ROSAT ($E \approx 100\text{-}284$ eV). In all cases the emission is sharply peaked near the center of the galaxy and drops off quickly with galactocentric radius. For our standard case ($n_a = 0.1 \text{ cm}^{-3}$, no conduction) we find in the R12L band a rate of 550×10^{-6} counts $\text{s}^{-1} \text{ arcmin}^{-2}$ (this is the standard unit for such ROSAT observations). Comparing this result to the surface brightness measured by CSM at the boundary between rings 2 and 3 (which corresponds approximately to the Solar Circle), we find that our result lies below the 95% upper limits for all the galaxies observed, and above the 95% confidence lower limits for all but two of the galaxies listed, namely NGC 4736 and NGC 5055. The fact that we get agreement with the observations, despite the large luminosity is a result of the softness of our spectrum. As has been pointed out previously (Cox & McCammon 1986), the relative faintness of the observed soft X-rays from external galaxies requires that much of the supernova energy is absorbed in the disk. Our model provides a natural explanation of why that occurs. Most of the radiated supernova energy is generated at low energies (see Figure 1) and few of the photons escape.

3. Photoionization Due to the Hot Gas Emission

Soft X-ray/EUV photons that are radiated by hot gas from SNRs will either be absorbed or escape the galaxy. Since the mean half-thickness of the disk is $N_{\text{H}0} \sim 3 \times 10^{20} \text{ cm}^{-2}$, nearly all of the ionizing photons less energetic than 0.5 keV will be absorbed. The surprisingly low soft X-ray brightness observed for external galaxies (CSM) is an indication that a large fraction of the X-rays generated by SNRs are being retained by the galaxies and therefore should contribute to their ionization. The photoionization rate of species i per unit area of disk is then

$$\zeta_{iA} = \int_{\nu_i}^{\infty} d\nu (1 - \eta_\nu) \left(\frac{\sigma_{i\nu}}{\sigma_\nu} \right) \frac{\langle \epsilon_{\nu A} \rangle}{h\nu}, \quad (7)$$

$$\simeq y_i \int_{\nu_i}^{\infty} d\nu \frac{\langle \epsilon_{\nu A} \rangle}{h\nu}, \quad (8)$$

since $\eta_\nu \simeq 0$; here ν_i is the frequency threshold for ionization of species i and y_i is the fraction of the photons absorbed by species i . For hydrogen, y_{H} is very close to unity since almost every helium ionization results in the emission of a hydrogen ionizing photon (Osterbrock 1989); for helium, $y_{\text{He}^0} \sim 0.6$ in weakly ionized regions since hydrogen competes for the ionizing photons. Defining $\langle \epsilon_{iA}^* \rangle \equiv \int_{\nu_i}^{\infty} d\nu \langle \epsilon_{\nu A} \rangle / h\nu$, which is the rate of generation of photons with $\nu \geq \nu_i$ per unit area, we

can express the ionization equation as simply

$$\zeta_{iA} = y_i \langle \epsilon_{iA}^* \rangle. \quad (9)$$

Note that here and below we use the superscript (*) to denote units of photons instead of units of energy; this should not be confused with the conventional notation for absorption lines from excited fine structure states, such as C^{+*} . The ionization rate is thus almost independent of the morphology of the $N(\text{H I})$ distribution—it does not matter whether the H^0 is in small, optically thin clouds or large optically thick slabs (for helium, there can be a weak dependence of y_{He^0} on the cloud morphology). The ionization of hydrogen determines the emission measure

$$EM_{\perp\text{pc}} = \frac{\langle \epsilon_{\text{HA}}^* \rangle}{\alpha_{\text{H}}^{(2)}} = 1.25 \times 10^{-6} T_4^{0.8} \langle \epsilon_{\text{HA}}^* \rangle \text{ cm}^{-6} \text{ pc} \quad (10)$$

from equation (A12). The subscript “pc” on $EM_{\perp\text{pc}}$ indicates that it is measured in units of cm^{-6} pc; $\langle \epsilon_{\text{HA}}^* \rangle$ has units photons $\text{cm}^{-2} \text{ s}^{-1}$; and $EM_{\perp\text{pc}}$ is the emission measure normal to the plane of the galaxy and through the entire disk. Photoionization by emission from hot gas thus sets a floor on the emission measure that should be observable on nearly all lines of sight.

To relate the ionization rate to the properties of individual SNRs, we define

$$\phi(> \nu_i) \equiv \int_{\nu_i}^{\infty} d\nu \phi_{\nu} \quad (11)$$

as the fraction of the SN energy emitted above ν_i and

$$\frac{1}{h\bar{\nu}_i} \equiv \frac{1}{\phi(> \nu_i)} \int_{\nu_i}^{\infty} d\nu \frac{\phi_{\nu}}{h\nu} \quad (12)$$

is the inverse of the mean energy of ionizing photons for species i . In terms of these quantities, the number of photons emitted above ν_i by an SNR is

$$\mathcal{N}_{\gamma}(> \nu_i) = \frac{\phi(> \nu_i) E_{\text{SN}}}{h\bar{\nu}_i} = 4.6 \times 10^{61} \phi(> \nu_i) \left[\frac{E_{\text{SN}}}{10^{51} \text{ erg}} \right] \left[\frac{13.6 \text{ eV}}{h\bar{\nu}_i} \right], \quad (13)$$

and the rate of generation of ionizing photons per unit area is

$$\langle \epsilon_{iA}^* \rangle = S_A \mathcal{N}_{\gamma}(> \nu_i) \quad (14)$$

$$= 1.26 \times 10^6 \left(\frac{S_A}{3.8 \times 10^{-5} \text{ kpc}^{-2} \text{ yr}^{-1}} \right) \left[\frac{\mathcal{N}_{\gamma}(> \nu_i)}{10^{61} \text{ photons}} \right] \text{ photons cm}^{-2} \text{ s}^{-1}. \quad (15)$$

In Table 1 we illustrate the nature of the spectrum emitted by SNR for the different model assumptions by listing the fraction of the SN energy emitted in several different energy bands and the commonly used ionizing photon ratio, $Q(\text{He}^0)/Q(\text{H}^0)$. This latter is the ratio of the total number of He^0 ionizing photons to H^0 ionizing photons emitted. The energy bands are defined as follow: ϕ_{H} : 13.6–24.6 eV, ϕ_{He^0} : 24.6–54.4 eV, ϕ_{He^+} : 54.4–284 eV, ϕ_{X} : > 284 eV. The first two are defined by the hydrogen and helium ionization edges. The edge at 284 eV is the carbon edge above which

C and other elements are responsible for a significant amount of the opacity. The C edge also corresponds (not coincidentally) to the cutoff in response in the Wisconsin C band and the *ROSAT* R1 and R2 bands. It is clear that while there is a general trend towards harder spectra for SNR expanding in higher ambient density, n_a , the trend is not monotonic in all the energy bands. This is due to fact that the emission spectrum is line-dominated so that a few strong lines from ions of an abundant element can substantially affect the total emission within an energy band.

Table 2 lists the emission measures generated by our modeled SNRs, together with characteristics of the ionizing spectrum, for several values of the ambient density and thermal conductivity. We have assumed $T = 8000$ K in evaluating the emission measure, and we have divided the value given in equation (10) by 2 in order to give the value that would be measured from the midplane of the disk. Typically somewhat more than half the energy of a SNR is emitted in ionizing photons, and the mean energy of these photons is only about 20 eV.

The effects on the spectrum of varying conductivity are quite small, despite the fact that the temperature at the center of the remnant is radically different for the two cases. When thermal conduction is included, the central temperature flattens quickly and the thermal energy is shared with matter further out in the remnant. The effects on the emission are small, however, because the emissivity is sharply peaked towards the edge of the remnant where the temperature and density profiles are little effected by conduction.

The effects of varying the ambient density are similarly small. To first order, the luminosity, spectrum, and EM are independent of n_a . However, as can be seen from Tables 1 and 2, there is a weak trend in that higher ambient density leads to slightly harder emission spectrum. This is due to the fact that a supernova remnant evolving in a higher density medium becomes radiative earlier, when the gas inside is at a higher temperature. Since the radiative phase is the period of greatest luminosity for the remnant, this has an effect on the mean emissivity even though the radiative phase lasts for only a small fraction of the remnant lifetime. The differences in the hardness of the spectrum for the different cases can be seen both from the mean energy of ionizing photons and the fraction of the emitted energy in ionizing photons.

It is noteworthy that while the ambient density in our models varies by a factor of 25, the emission measure generated for the extreme cases differ by only 34%. The intensity of an H α line in Rayleighs is related to the emission measure by $I^*(\text{H}\alpha) = 0.445EM_{\text{pc}}$ R for $T = 8000$ K from equation (A14). (Note that although the relation between I^* and EM depends on temperature, the relation of I^* to the underlying emissivity $\langle\epsilon_{\text{HA}}^*\rangle$ is almost independent of temperature—see eq. A15.) Our standard model gives $(EM_{\perp\text{pc}}/2) = 1.2 \text{ cm}^{-6} \text{ pc}$ for the half disk, which corresponds to a predicted intensity at $b = 90^\circ$ of $I^*(\text{H}\alpha) = 0.53$ R. By comparison, Reynolds (1991) has suggested 1 R as a “typical” minimum value for the diffuse H α background at $b = 90^\circ$, with the emission roughly following a $\csc b$ law. Those conclusions were based on a sampling of regions observed at moderately high latitudes using a less sensitive instrument than the current instrument, WHAM (Wisconsin H α Mapper). Even those data showed substantial variation in the value of $I \sin b$,

and more recent data reveal the existence of many regions of low emission, well below the 1 R zenith value of the earlier estimate. One of these is the direction towards HD 93521 discussed in detail below. Thus, SNRs are capable of accounting for the observed H α intensity in at least some directions in the halo. It is clear that the cooling hot gas in our model makes a substantial contribution to the ionization of hydrogen in the warm ionized medium of our galaxy and sets a lower limit on the ionization.

Another way of testing our model is to compare it to the ionization of other elements. Absorption line data provide particularly good tests since high spectral resolution observations allow us to separate different velocity components and thus model individual clouds. A particularly useful example is the line of sight towards HD 93521.

4. The HD 93521 Line of Sight

4.1. The Data

The line of sight towards the halo star HD 93521 ($\ell = 183^\circ, b = 62^\circ$), while in some ways quite unusual, reveals important information about the background ionizing radiation field in the galaxy. The line of sight is unusual in two ways. First, there appear to be no stars close enough to it to be significant ionizing sources (with the exception, of course, of HD 93521 itself, which could ionize no more than one of the clouds, see below). Note that it is not unusual for any given point in the galaxy to be far from O stars, rather it is the fact that the entire 1.7 kpc line of sight is far from any O stars that makes it somewhat exceptional. This can be seen by examining figure 16 (particularly 16a and 16b) of Miller & Cox (1993). In that figure, they present the outlines of the extended H II regions resulting from the observed distribution of nearby O stars. The line of sight does not pass through any of the H II regions, reflecting the fact that no O stars are close to the line of sight. [Note: in figure 16c the Sun and the line of sight towards HD 93521 appear to be on the edge of an H II region. It is unclear which star might be responsible for this ionization (perhaps ζ Oph) and it is unlikely to be capable of ionizing clouds towards HD 93521.] Secondly, observations by Spitzer & Fitzpatrick (1993, hereafter SF) show that there is extremely little cold neutral gas along the line of sight. Thus we have in this line of sight an excellent opportunity to observe ionization of warm diffuse gas by non-stellar sources without confusion by interspersed cold gas.

The absorption line data for HD 93521, including lines of S II, S III, C II*, and several other lines, reveal a number of velocity resolved features, or “clouds”, all indicating partial ionization (SF). Complementing the absorption line data are new observations using the Wisconsin H α Mapper (WHAM; Reynolds et al. 1998) of diffuse emission in H α , [N II] $\lambda 6584$, and [S II] $\lambda 6716$ (Pifer et al. 1999). The velocity components in the absorption lines split roughly into two groups of 4 clouds each, the “fast” clouds with $-70 \text{ km s}^{-1} < v_{\text{LSR}} < -30 \text{ km s}^{-1}$ and the “slow” clouds with $-20 \text{ km s}^{-1} < v_{\text{LSR}} < 10 \text{ km s}^{-1}$. The emission lines cannot be resolved into individual cloud components at this time, but they do split up into broad “fast” and “slow” compo-

nents that correspond to the absorption line groups. Hausen et al. (1999) find that for the slow clouds, $I^*(\text{H}\alpha) = 0.22 \pm 0.06 \text{ R}$, and for fast clouds, $I^*(\text{H}\alpha) = 0.16 \pm 0.03 \text{ R}$. Pifer et al. (1999) find $I^*([\text{N II}] \lambda 6584) = 0.22 \text{ R}$ for the slow clouds and 0.29 R for the fast ones; they also find $I^*([\text{S II}] \lambda 6716) = 0.24 \text{ R}$ for the slow clouds and 0.19 R for the fast ones (see Table 3).

4.2. Modeling the Ionization

In order to calculate the ionization of clouds subjected to the SNR-generated flux of our model (Figure 1) we make use of the photoionization/thermal equilibrium code CLOUDY (Ferland 1996). The flux has been scaled by reducing S_A by 0.68 in order to give the observed value for the $\text{H}\alpha$ intensity. In order to approximate the effect of isotropic, diffuse radiation using CLOUDY, which is designed for point source calculations, we use the “illuminate” command with the parameter value 60, which simulates flux coming into the cloud face at an angle of 60 degrees. We also use the “case b” command to avoid the artificial excitation of $\text{H}\alpha$ emission due to absorption of FUV background photons at Lyman β . We use a fixed temperature and have explored a range from 6000 K to 9000 K. Fixed T avoids the complications of heating/cooling balance that involve the amount of dust heating (particularly due to PAHs) (Bakes & Tielens 1998), which is only crudely included in the code, and the uncertain details of the elemental abundances. We discuss heating further below.

Although the usual approach is to assume that individual velocity features are physical “clouds”, we examined the possibility that the features were actually formed from collections of smaller clouds or “cloudlets”. This affects the opacity of the medium and thus the hardness of the radiation field incident on a typical cloud, but it does not affect the emission measure along the line of sight since nearly all ionizing photons are absorbed somewhere in the disk. The difference between many small cloudlets and a few big clouds is greatest near the Lyman limit, where for small cloudlets the incident flux is much less. We have constructed two models to try to differentiate between these two cases. The “cloudlet” model has cloudlet column densities of $N_{\text{H}0} = 7 \times 10^{17} \text{ cm}^{-2}$. The simple cloud model has $N_{\text{H}0} = 1.46 \times 10^{19} \text{ cm}^{-2}$, the mean for the observed clouds towards HD 93521. The only data we have found that differentiates these two fairly extreme cases from each other is the ratio of $N_{\text{S}++}/N_{\text{S}+}$. This ratio has unfortunately only been observed for the fast clouds, but if we assume that the fast and slow clouds are at least geometrically similar (which might be doubtful, see below), then our results favor larger clouds over cloudlets. This is best seen by forming a ratio that is insensitive to the pressure of the clouds but still sensitive to the cloud size, $(N_{\text{S}++}/N_{\text{S}+}) \times (N_{\text{C}+*}/N_{\text{S}})$, where $N_{\text{S}} \simeq N_{\text{S}+} + N_{\text{S}++}$ to good accuracy. The lack of sensitivity to pressure derives from the fact that $N_{\text{S}++}/N_{\text{S}+}$ goes as $1/n_e$ (for a fixed input spectrum), while $N_{\text{C}+*}/N_{\text{S}}$ goes as n_e . Comparing this ratio for both cloud size assumptions, we find that the cloudlet model results in too low a ratio, ~ 0.0007 , whereas the larger clouds yield a ratio of ~ 0.002 , close to the observed values. For this reason, and because of the various conceptual difficulties inherent in the cloudlet picture, we have focussed our attention on the more standard cloud picture (i.e. velocity features corresponding to spatially coherent clouds) in our comparisons with the data. It

should be noted, however, that lacking the SIII line observations for the slow clouds, we are unable to differentiate between the cloud size models for those clouds.

Up to this point we have not discussed the ionization due to HD 93521 itself. According to Vacca, Garmany & Shull (1996), HD 93521, an O9.5V star, should have a luminosity in ionizing photons of $2.40 \times 10^{48} \text{ s}^{-1}$. This then implies that the star can create enough ionization to produce $I^*(\text{H}\alpha) = 9320/r_{\text{pc}}^2$ Rayleigh from equation (A15), where r_{pc} is the distance of the cloud from the star in pc. We do not have any direct information on the distance between HD 93521 and the cloud nearest to it. HD 93521 is determined to be at a height above the plane of $z \simeq 1500 \text{ pc}$, well above scale height of neutral and even ionized gas. From this we estimate that the contribution of HD 93521 to the H α observed towards it is $\lesssim 10\%$. In any case, since all the clouds observed by SF are optically thick in the EUV, the first cloud along the line of sight will absorb all the ionizing radiation and the other clouds are not affected by HD 93521. We do not include its contribution to the ionization in our calculations.

4.3. Model Results

Our model results for both the absorption lines and emission lines, combined into “fast” and “slow” cloud groups are compared with the observations in Table 3. We use results from a series of CLOUDY runs with the same input spectrum (SNR model with $n_a = 0.1$, $E_0 = 10^{51}$ ergs, no conduction) and pressures ranging from $P/k = 1000\text{--}2 \times 10^4 \text{ cm}^{-3} \text{ K}$. The model value for the observed column densities and intensities for each cloud is determined by finding which pressure value led to the best match with the observed C II*/S II line ratio at the observed value of N_{S^+} . We then use the results of the best match pressure run for determining the values for the other observables. We choose to peg our results to the C II*/S II line ratio because it is one of the best determined observationally for the line of sight.

Because we fix the other quantities calculated in our models by their values at the observed N_{S^+} values for each cloud, the model and observed values for N_{S^+} are identical. We also match the total line of sight (fast+slow) value for H α intensity by scaling the input spectrum as described in §3. The model values for $N(\text{C II}^*)$ are also very close to the observed values, as a result of our fixing the pressure value by finding the best match for the C II*/S II line ratio as described above. Thus the first three lines of the table constitute inputs for the model. For the rest of the table, the model results are truly outputs, not having been fixed to match the data. For these results (as well as for $N_{\text{C}^{++}}$ for completeness) we have presented ranges for the model results corresponding to a (fixed) cloud temperature of 6000 K and 8000 K respectively. This range of values might correspond to the temperatures in the neutral and ionized portions of the clouds as we discuss below.

One of the most confusing aspects of the absorption line data is the apparently large neutral column densities of the clouds, as seen in either H I or S II, coupled with large ionized columns, as inferred from the relatively high columns of C^{++} , which is mainly excited by collisions with electrons

in diffuse, $n \approx 0.2 \text{ cm}^{-3}$ gas. This is especially true for the slow clouds. If one interprets each velocity component as being due to a partially ionized cloud, these data require either a very large ionizing flux and/or a high thermal pressure. As we discuss in more detail below, this is because $N_{\text{C}^{+*}}/N_{\text{H}^0} \sim xn/(1-x)$, where $x \equiv n_{\text{H}^+}/n$ is the fractional ionization of hydrogen. The observed values of $N_{\text{C}^{+*}}/N_{\text{H}^0}$ imply high values for x and/or n for the clouds at the same time that N_{H^0} is large ($3 \times 10^{18} - 2 \times 10^{19} \text{ cm}^{-2}$).

The $\text{H}\alpha$ data taken with WHAM (Hausen et al. 1999), however, provide tight limits on the ionizing flux. For an assumed temperature of 8000 K, their data imply an emission measure of $0.85 \text{ cm}^{-6} \text{ pc}$ for this line of sight. With the added information from the emission measure ruling out a very large photoionizing flux, we are faced with the prospect of large thermal pressures in the slow clouds. This is demonstrated in figure 2, where we plot the $N_{\text{C}^{+*}}/N_{\text{S}^+}$ ratio based on calculations using our model flux. The flux, which is assumed to be the same for all the clouds, has been adjusted to match the total $\text{H}\alpha$ intensity observed for the line of sight. For our standard model this required reducing the flux by a factor of 0.68. The x -axis is the total thickness of a cloud, as opposed to depth into a cloud. The points are labelled as in SF but with cloud no. 5 (the smallest and most poorly detected component) excluded. The fast clouds are numbered 1–4 while the slow clouds are 6–9. We are able to match the observed ratios fairly well, although rather high thermal pressures are demanded for the slow clouds, $P/k \approx 7500 - 2 \times 10^4 \text{ cm}^{-3} \text{ K}$. There is evidence that in regions as diverse as the fairly quiescent hot gas of the Local Bubble and the cold neutral gas at greater distances (Jenkins, Jura & Loewenstein 1983), high thermal pressures, $P/k \sim 10^4 - 2 \times 10^4 \text{ cm}^{-3} \text{ K}$, do exist in the ISM. A difficulty with the high value of the inferred pressure, however, is that it could lead to more cooling than can be balanced by the known available heating sources at $T \sim 7000 \text{ K}$, which would transform the cloud from the warm phase to the cold phase. We discuss the problem with the heating/cooling balance further below in §6.2.

The reason for the high pressures demanded for the slow clouds can be seen analytically (see also McKee & Slavin 1999, for a more extensive discussion). Under the assumption of uniform ionization and temperature (as used by SF), the ratio of $\text{H}\alpha$ intensity to C^{+*} column density gives the hydrogen ionization fraction, x ,

$$\frac{I^*(\text{H}\alpha)}{N_{\text{C}^{+*}}} = \frac{\alpha_{\text{H}\alpha}(T)A_{21}}{10^6 \mathcal{A}_{\text{Cg}}\gamma_{12}} x, \quad (16)$$

where $\alpha_{\text{H}\alpha}$ is the effective recombination coefficient for emission of $\text{H}\alpha$ (see the Appendix), \mathcal{A}_{Cg} is the abundance of gaseous carbon, γ_{12} is rate coefficient for excitation of C^+ to the $J = 3/2$ level and A_{21} is the downward transition probability. $I^*(\text{H}\alpha)$ is assumed to be in Rayleighs and gaseous carbon is assumed to be entirely singly ionized. Applying equation (16) to the data towards HD 93521 (and assuming a temperature of 8000 K) yields $x = 0.37 \pm 0.075$ and $x = 0.14 \pm 0.038$ for the fast and slow clouds, respectively. (Note that the temperature of 8000 K was used here rather than the 6000 K of SF because of results from recent emission line measurements that we discuss below.) This estimate of the ionization can then be used with the observations of the H I column

densities to get constraints on the pressure. Assuming that H and He are equally ionized we derive

$$\frac{N_{\text{C}^{+*}}}{N_{\text{H}^0}} \approx \left(\frac{P}{kT} \right) \frac{\gamma_{12}}{A_{21}} \mathcal{A}_{\text{Cg}} \left(\frac{x}{1-x^2} \right). \quad (17)$$

Using our results from above this implies (again assuming $T = 8000$ K) $P/k = 1120 \pm 340$ and 9220 ± 2770 for the fast and slow clouds, respectively, where most of the uncertainty derives from the $\sim 20\%$ uncertainty in the $\text{H}\alpha$ intensities. For the more realistic case in which ionization varies with depth into the cloud, as in our model, the value of x derived in equation (16) is weighted by n_e , thereby emphasizing the most highly ionized part of the cloud. As a result, the true mean ionization will be less than that estimated assuming uniform ionization. Equation (17) carries with it a different weighting of x , introducing more uncertainty in the determination of P . Again the effect is to emphasize regions of higher ionization resulting in an *underestimate* of the pressure. Despite these limitations we infer that the fast and slow clouds are markedly different in their mean ionization level and their pressures. The slow clouds have high thermal pressures, $\sim 10^4 \text{ cm}^{-3} \text{ K}$. The fast clouds are more highly ionized and have lower thermal pressures, $P/k \sim 2000 \text{ cm}^{-3} \text{ K}$, more typical of diffuse interstellar clouds (Jenkins, Jura & Loewenstein 1983).

As detailed above, we have no difficulty matching the observed $\text{H}\alpha$ intensities towards HD 93521. The other emission line data, observations of $[\text{S II}] \lambda 6716$ and $[\text{N II}] \lambda 6584$ (Pifer et al. 1999), are more problematic, however. These data are consistent with the trend recently discovered in the new WHAM data (e.g. Hausen et al. 1999) of both $[\text{S II}]/\text{H}\alpha$ and $[\text{N II}]/\text{H}\alpha$ to increase to high values as $\text{H}\alpha$ decreases and as galactic latitude increases. The values for these ratios are a factor of 3 or more larger than is typical for diffuse emission in the galactic plane. The $[\text{N II}]/\text{H}\alpha$ ratio is a good temperature diagnostic since the ionization potentials of hydrogen and nitrogen are within 1 eV of each other. The reported values for $I(6584)/I(\text{H}\alpha)$ of 1 and 1.8 (for the slow and fast clouds respectively) demand high temperatures, $T \approx 8000$ K and $T \gtrsim 9000$ K. Another temperature diagnostic is the $N_{\text{C}^{+*}}/I([\text{S II}])$ ratio, because $N_{\text{C}^{+*}}$ is relatively insensitive to T whereas $[\text{S II}]$ increases rapidly with rising T . Since both C^+ and S^+ are expected to be the dominant stages of ionization in WIM/WNM gas, both quantities in the ratio go as $\sim n_e n_{\text{H}}$ and the density dependence cancels in the ratio. In contrast to $[\text{N II}]/\text{H}\alpha$, however, the observed values for $N_{\text{C}^{+*}}/I([\text{S II}])$ indicate relatively low temperatures, $T < 6000$ K for the slow clouds and $T \approx 7000$ K for the fast clouds. A potential solution to this seeming contradiction is to have substantially lower temperatures in the neutral regions of the clouds relative to the ionized regions. $I(6584)$ and $I(\text{H}\alpha)$ are weighted towards the ionized part of the cloud (both the H^+ and N^+ densities are highest there), while $N_{\text{C}^{+*}}$ and $I([\text{S II}])$ have greater contributions from the neutral part of the clouds. As we noted above, we are unable to model the thermal structure of the WIM/WNM accurately using CLOUDY because it does not yet include PAH heating accurately. Calculations by Wolfire et al (1995a) indicate that temperatures in the WNM range from ~ 5000 – 9000 K depending on various model parameters including the assumed pressure. Higher pressures lead to lower temperatures which is consistent with the observation that the high pressure, slow clouds have a high $N_{\text{C}^{+*}}/I([\text{S II}])$ ratio while the lower pressure, fast clouds have a lower $N_{\text{C}^{+*}}/I([\text{S II}])$ ratio. In summary, it appears that the

slow clouds have $T \sim 5000$ K in the more neutral regions and $T \sim 8000$ K in the more highly ionized regions, while the fast clouds are characterized by $T \sim 7000$ K in the more neutral regions to $T \sim 9000$ K in the more ionized regions.

One additional output from our modeling of the clouds is the filling factor of cloud material. This is more clearly stated in terms of the total line of sight distance occupied by the clouds as determined by their densities and column densities. For our “best fit” models as described above we find that the clouds account for only 100–150 pc of the ~ 1700 pc line of sight towards HD 93521. Thus only 6–9% of the line of sight is occupied by the warm ionized and neutral gas. It is likely that this is not evenly distributed but rather that there are more clouds near the plane. Nevertheless, even assuming the clouds are confined within 1 kpc of the galactic plane their filling factor would only be 9–13%. Thus for this low column density, high latitude line of sight, warm diffuse gas appears to have a low filling factor.

5. Helium Ionization and the X-ray Opacity of the Halo

A possible constraint on the nature of the ionizing flux in the halo comes from the recent study of the halo’s X-ray opacity by Arabadjis & Bregman (1999, hereafter A&B). A&B inferred the opacity τ in Galactic gas needed to account for the X-ray spectra of a number of galaxy clusters (including 13 at high latitude) observed with *ROSAT*. In each case, they determined an effective H^0 absorption column density $N_{\text{H},X}$ based on the assumptions that the absorbing gas is neutral and contains 10% helium by number,

$$\tau \equiv N_{\text{H},X}(\sigma_{\text{H}^0} + 0.1\sigma_{\text{He}^0}), \quad (18)$$

where the cross sections, σ_{H^0} and σ_{He^0} are evaluated at the energy appropriate to the X-ray observations, 0.25 keV. They then compared these column densities with those determined directly from 21 cm observations, N_{H^0} (which they termed $N_{\text{H},21\text{cm}}$). Because the values of $N_{\text{H},X}$ make no allowance for ionized gas, which presumably contains some neutral and once ionized helium, one would expect $N_{\text{H},X}$ to be substantially larger than the actual N_{H^0} . What they found instead was that for the low column, high latitude directions, $\langle N_{\text{H},X}/N_{\text{H}^0} \rangle = 0.972 \pm 0.022$.

As A&B pointed out, this result is difficult to understand. The two column densities are related by

$$N_{\text{H},X}(\sigma_{\text{H}^0} + 0.1\sigma_{\text{He}^0}) = N_{\text{H}^0}\sigma_{\text{H}^0} + N_{\text{He}^0}\sigma_{\text{He}^0} + N_{\text{He}^+}\sigma_{\text{He}^+}, \quad (19)$$

where at the typical energy of the observations (0.25 keV), the cross sections are $\sigma_{\text{H}^0} = 1.08 \times 10^{-21}$ cm^{-2} , $\sigma_{\text{He}^0} = 2.81 \times 10^{-20}$ cm^{-2} , and $\sigma_{\text{He}^+} = 2.04 \times 10^{-20}$ cm^{-2} . Following A&B, we define $C \equiv N_{\text{H},X}/N_{\text{H}^0}$. Let x_{He} be the helium abundance relative to hydrogen, and let $\chi_{\text{H}^+} \equiv N_{\text{H}^+}/N_{\text{H}}$, $\chi_{\text{He}^+} \equiv N_{\text{He}^+}/N_{\text{He}}$, etc, be the fractional ionizations averaged along the line of sight. Inserting the values of the cross sections, we obtain

$$C = 0.278 + \frac{0.722}{1 - \chi_{\text{H}^+}} \left(\frac{x_{\text{He}}}{0.1} \right) (1 - 0.274\chi_{\text{He}^+} - \chi_{\text{He}^{++}}). \quad (20)$$

A&B adopted $\chi_{\text{H}^+} = 0.27$ and $\chi_{\text{He}^+} = 0.5\chi_{\text{H}^+}$ for the ISM at the solar circle, which gives $C = 1.23$ for a helium abundance $x_{\text{He}} = 0.1$. If the helium abundance were $x_{\text{He}} = 0.09$, as suggested by Baldwin et al (1991) in their analysis of the Orion Nebula, then $C = 1.14$. Neither value comes close to matching the observed value, $C = 0.972$.

Our analysis of the line of sight toward HD 93521 gives a significantly lower hydrogen ionization than adopted by A&B, $\chi_{\text{H}^+} = 0.18$, but a comparable helium ionization, $\chi_{\text{He}^+} = 0.15$. The column density of doubly ionized helium is negligible, $\chi_{\text{He}^{++}} = 0.0017$. The difference in the hydrogen ionization fractions is due in part to the fact that the fully ionized HIM does not enter into our analysis, whereas it does contribute to pulsar dispersion measures (Wolfire et al 1995b) and thus to the value of N_{H^+} used by A&B, as they recognized. Our lower hydrogen ionization gives lower values for C , 1.12 and 1.04 for $x_{\text{He}} = 0.1$ and 0.09, respectively. In view of the many possible systematic effects that could enter into determining C observationally, we do not regard the discrepancy between our model and A&B’s observation as significant.

6. Discussion

6.1. The Calculated Spectrum

The main results of this paper involve the ionization caused by cooling hot gas from supernova remnants. Thus questions of the accuracy of the spectra we have produced are of central importance. There are two concerns in this regard: the supernova remnant evolution model and the plasma emission model.

It is clear that our SNR models are highly simplified. In reality, SNRs evolve in a very inhomogenous medium that contains material with a wide range of densities, ionization states, magnetic field strengths and temperatures. In the case of type II and type Ibc supernovae, the stellar progenitor will have shaped the medium into which the remnant evolves. The magnetic field in the ISM can have important influences on the radiative properties of remnants by limiting the compression in the cold shell that is formed during the radiative phase (Slavin & Cox 1992, 1993). Supernovae in OB associations combine to form superbubbles that can grow to kpc size, sometimes venting their hot gas into the halo. We justify the simplifications we have made by appealing to our results. Despite the drastically different temperature and density profiles that we see for the range of parameter values we explore ($n_a = 0.04\text{--}1.0 \text{ cm}^{-3}$; conduction turned on or off), the time-averaged spectra are not radically different. Over its lifetime, the hot gas radiates its energy primarily in the same lines in all cases, though differences in ionization and temperature shift the balance from one set of lines to another for the different cases. Because we are concerned with the time and volume averaged spectrum, the substantial differences between remnants at any given time in their evolution is smoothed out. Thus, while a strong magnetic field can cause a delay in the radiation from a SNR, we do not expect the time and space averaged spectrum to be substantially different from the spectrum for the no field case.

The reliability of the plasma emission code that we use, the “Raymond & Smith” code, is currently an area of active study. Soon more up-to-date and detailed plasma emission codes will become available (see Brickhouse 1999). The computed emission spectra and even the total cooling rates of hot plasmas using these codes may differ significantly from those calculated using the R&S code. However, for the reasons discussed in the preceding paragraph, the photoionization rates of the time and space averaged spectra will likely not be substantially changed.

A potentially more important limitation of the calculations we have presented is the lack of inclusion of interface radiation generated in the boundaries between cold and hot gas. Both thermal evaporation (McKee & Cowie 1977) and turbulent mixing (Slavin, Shull & Begelman 1993) at those boundaries could lead significant enhancement of cooling in those regions as well as an emission spectrum that is spectrally different from those that we have presented here. It is unclear at this time what fraction of the energy radiated by SNRs could be emitted in such interface regions. This is a worthy subject for future investigations.

6.2. Ionization and Thermal Balance in the Clouds

An important difficulty for our modeling of the clouds towards HD 93521 concerns the heating/cooling balance. As we mentioned in our description of our model, we chose to use a constant temperature in the clouds to avoid the sensitivity to gas phase elemental abundances and dust heating rates in our cloud modeling. Nevertheless, we have used CLOUDY, to examine the thermal balance in the gas for some cases of interest. We have found that, while at low pressure ($P/k = 1000\text{--}2000 \text{ cm}^{-3} \text{ K}$) CLOUDY can produce temperatures in the 5000–8000 K range in the ionized portion of the clouds, it has insufficient heating to maintain temperatures above 1000 K in the neutral portions of the cloud. For the low pressure (fast) clouds, we attribute this to the grain photoelectric heating model in CLOUDY. Using the best grain heating rates available, Wolfire et al (1995a) have shown that WNM (i.e, warm, $\sim 7000 \text{ K}$, neutral medium) can be maintained by dust and PAH heating at these pressures. However, the slow clouds have large neutral hydrogen column densities, and, from our modeling of the C II*, large pressures. Wolfire et al. also showed that the WNM cannot be maintained at pressures above $10^4 \text{ cm}^{-3} \text{ K}$, as seems to be demanded for some of the clouds. This difficulty can be ameliorated, but not entirely solved, if the slow clouds are broken up into small cloudlets. The cloudlet model has the advantage that, because of the low column density in an individual cloudlet, the ionization is more uniform. As discussed in §4.3, more uniform ionization decreases the pressure required to produce the observed $N_{\text{C}^{++}}/N_{\text{H}^0}$. However, Eq. (17) demonstrates that even under the extreme assumption of uniform ionization, fairly high pressures are demanded for the slow clouds, $P/k \sim 10^4 \text{ cm}^{-3} \text{ K}$. Some additional heating source seems to be needed to maintain these clouds at their observed temperatures of $\sim 6000\text{--}8000 \text{ K}$. Reynolds, Haffner & Tufte (1999) have also presented evidence from the WHAM survey for an additional heating mechanism in the halo. Some possibilities for such a heating source include photoelectric heating by small dust grains (Reynolds & Cox 1992), magnetic reconnection heating (Raymond

1992; Birk, Lesch & Neukirch 1998) and dissipation of turbulence (Minter & Balsaer 1998).

Another proposed source of ionization for the WIM is radiation from decaying neutrinos (Sciama 1990). This source was seen to have the advantage that, because neutrinos are essentially uniformly distributed throughout the Galaxy, the ionization rate per unit volume is nearly constant. Thus, clouds with large H I columns could be evenly and partially ionized throughout. There are several difficulties with this, however, that make neutrinos a very unlikely candidate for the ionization of the clouds towards HD 93521. First, we have identified a source of ionization associated with the *observed* X-ray background that can account for essentially all the ionization observed along this line of sight. While the details in our model can be improved upon by using more realistic models for the evolution of supernova remnants and for the structure of the ISM, it is difficult to escape the conclusion that the Galactic X-ray background has a low energy tail that can produce significant photoionization. Second, the photon energy from the decaying neutrinos is estimated to be only about 13.7 eV (Sciama 1995), which is inadequate to account for the observed N^+ (Pifer et al. 1999) or S^{++} (Spitzer & Fitzpatrick 1993). Thus another source capable of creating these ions is needed in any case, and this source will ionize hydrogen as well. Finally, we note that we find, in agreement with Reynolds (1991) and Spitzer & Fitzpatrick (1993), that most of the volume along the line of sight to HD 93521 is apparently empty. In Sciama’s (1997) model, however, much of this volume is filled with gas that is maintained in a fully ionized state by the decaying neutrinos. This gas should have detectable absorption lines, but none were found by Spitzer & Fitzpatrick.

7. Conclusions

Ionization in the warm diffuse interstellar medium of our galaxy is substantially influenced by the soft X-ray/EUV emission from cooling hot gas in supernova remnants. In the galactic halo, hot gas emission is especially important, dominating the ionization in some regions. In this paper we have presented calculations of the spectrum from the cooling hot gas and the ionization that results. We have found that:

- the hot gas is capable of producing roughly 50% of the EM observed for a typical line of sight through the galactic disk, and more than enough to account for that observed toward HD 93521;
- our calculated spectrum is consistent with the observed soft X-ray diffuse background at high latitudes;
- the flux we calculate is also consistent with the soft X-ray emission observed from other spiral galaxies;
- we predict a low strength of the He I $\lambda 5876$ recombination line along the HD 93521 sight line, consistent with low values seen in large beam observations;

- the ionization in our models allows us to match the C^{+}/S^{+} and the S^{++}/S^{+} ratios seen with absorption measurements along the HD 93521 line of sight, though for the “slow” clouds large thermal pressures ($10^4 - 2 \times 10^4 \text{ cm}^{-3} \text{ K}$) are required;
- by varying the assumed temperature in our clouds from $\sim 6000 - 9000 \text{ K}$, we are able to match the observed emission line strengths of [S II] and [N II], and predict the intensity of [O I] $\lambda 6300$;
- with allowance for the uncertainty in the helium abundance and possible systematic effects in the analysis of the data, we regard our value for the X-ray opacity toward HD 93521 as being consistent with the value inferred by Arabadjis & Bregman (1999) for the halo;
- by accounting for the observed ionization toward HD 93521 with a theoretical extrapolation of a *known* source of ionization, the Galactic X-ray background, we obviate the need to invoke exotic ionization mechanisms such as decaying neutrinos (Sciama 1990).

We are thankful to Ron Reynolds, Steve Tufte, and Nancy Hausen for sharing their observational results with us prior to publication. We also thank Gary Ferland for discussions regarding CLOUDY and sulphur dielectronic recombination rates. We wish to recognize the contribution of Xander Tielens who participated in our early discussions of this project. CFM gratefully acknowledges support by an NSF grant (AST95-30480), a grant from the Guggenheim Foundation, and a grant from the Sloan Foundation to the Institute for Advanced Study. The authors acknowledge support from the NASA Astrophysical Theory Program.

A. TRANSFER OF IONIZING RADIATION IN THE HALO

In the absence of scattering, the equation of transfer is

$$\mu \frac{dI_\nu}{d\tau_\nu} = S_\nu - I_\nu, \quad (\text{A1})$$

in standard notation; recall that $S_\nu = j_\nu/\kappa_\nu$ is the source function. We model the disk and halo of a galaxy as having an emissivity j_ν and opacity κ_ν that depend only on the distance from the midplane, z . Solving this equation for the flux, $F_\nu \equiv \int \mu I_\nu d\Omega$, we find that the flux measured above the halo is

$$F_{\nu+} = F_{\nu-} + 4\pi \int_0^{\tau_{0\nu}} S_\nu d\tau_\nu - 4\pi \int_0^{\tau_{0\nu}} J_\nu d\tau_\nu, \quad (\text{A2})$$

where $F_{\nu-}$ is the flux measured below the halo, $J_\nu = (1/4\pi) \int I_\nu d\Omega$ is the mean intensity, and $\tau_{0\nu}$ is the total optical depth of the galaxy (measured normal to the plane). Note that $4\pi \int S_\nu d\tau_\nu = \int 4\pi j_\nu dz$ is the total emission per unit area. The expected value of j_ν is $\langle \epsilon_\nu \rangle / 4\pi$, where the expected

volume emissivity $\langle \epsilon_\nu \rangle$ is defined in equation (1). We define the emissivity per unit area as

$$\langle \epsilon_{\nu A} \rangle \equiv \int_{-\infty}^{\infty} dz \langle \epsilon_\nu \rangle = 4\pi \int_0^{\tau_{0\nu}} S_\nu d\tau_\nu. \quad (\text{A3})$$

The mean escape probability—i.e., the fraction of the radiation that escapes the galaxy—is

$$\eta_\nu = \frac{F_{\nu+} - F_{\nu-}}{4\pi \int_0^{\tau_{0\nu}} S_\nu d\tau_\nu} = \frac{F_{\nu+} - F_{\nu-}}{\langle \epsilon_{\nu A} \rangle}. \quad (\text{A4})$$

In terms of the mean escape probability, the mean value of the average intensity is

$$\bar{J}_\nu \equiv \frac{1}{\tau_{0\nu}} \int_0^{\tau_{0\nu}} J_\nu d\tau_\nu = \frac{(1 - \eta_\nu)}{\tau_{0\nu}} \int_0^{\tau_{0\nu}} S_\nu d\tau_\nu \quad (\text{A5})$$

from equation (A2), so that

$$\bar{J}_\nu = \frac{(1 - \eta_\nu)}{\tau_{0\nu}} \left(\frac{\langle \epsilon_{\nu A} \rangle}{4\pi} \right). \quad (\text{A6})$$

In order to calculate the mean escape probability, we must make an assumption about the spatial distribution of the emissivity and absorption. We make the simplest assumption possible: The source function is constant ($j_\nu \propto \kappa_\nu$). In that case, the flux escaping from the top of the halo is

$$F_{\nu+} = \int d\Omega \int_0^{\tau_{0\nu}} S_\nu e^{-\tau_\nu/\mu} d\tau_\nu = 2\pi S_\nu \int_0^1 d\mu \int_0^{\tau_{0\nu}} e^{-\tau_\nu/\mu} d\tau_\nu. \quad (\text{A7})$$

The magnitude of the flux escaping from the bottom of the halo is the same. Evaluating the integrals and using equation (6), we find

$$\eta_\nu = \frac{1}{\tau_{0\nu}} \left[\frac{1}{2} - E_3(\tau_{0\nu}) \right], \quad (\text{A8})$$

where E_3 is an exponential integral. Although we have numerically evaluated $E_3(\tau_{0\nu})$ in applying this equation in the text, it is sometimes useful to have an approximate analytic expression. The expression

$$\eta_\nu \simeq \frac{1}{1 + 2\tau_{0\nu}} \quad (\text{A9})$$

is accurate to within 20%, whereas the corresponding approximation for the absorbed fraction,

$$1 - \eta_\nu \simeq \frac{2\tau_{0\nu}}{1 + 2\tau_{0\nu}}, \quad (\text{A10})$$

has the same accuracy provided $\tau_{0\nu} > 0.03$. For ionizing photons with energies somewhat above 1 Ryd, the escape probability is small; as a result, the absorbed fraction is close to unity even if our assumption of a constant source function is badly violated, whereas the escaping fraction is quite sensitive to this assumption. For X-rays, the optical depth of the disk and halo is of order unity, so that the predicted X-ray luminosity of a galaxy is somewhat sensitive to the assumption of a constant source function.

A.1. Intensity of Recombination Lines

Essentially all the ionizing photons that are absorbed in the disk and halo ionize hydrogen; even those that initially ionize helium lead to the production of a hydrogen ionizing photon (Osterbrock 1989). If we ignore ionization by secondary electrons, the ionization equilibrium of hydrogen is governed by

$$\int_{\nu_H}^{\infty} d\nu (1 - \eta_\nu) \frac{\langle \epsilon_{\nu A} \rangle}{h\nu} = \alpha^{(2)} \int_{-\infty}^{\infty} dz n_e n_p = \alpha^{(2)} EM_{\perp}, \quad (\text{A11})$$

where $h\nu_H$ is the ionization potential of hydrogen, $\alpha^{(2)} \simeq 2.59 \times 10^{-13} T_4^{-0.8} \text{ cm}^3 \text{ s}^{-1}$ is the recombination coefficient to the excited states of hydrogen, and EM_{\perp} is the emission measure normal to the plane of the galaxy. Ionization by secondary electrons becomes dominant at large column densities (Maloney, Hollenbach & Tielens 1996), but for the relatively small column densities encountered in our model ($N \lesssim 1.5 \times 10^{19}$ —see §4), they contribute less than 2% to the emission measure based on calculations with CLOUDY. In fact, the escape probability is small for almost all the ionizing photons ($\eta_\nu \ll 1$), so the ionization balance can be approximately described by

$$\langle \epsilon_{\text{HA}}^* \rangle = \alpha^{(2)} EM_{\perp} = 7.99 \times 10^5 T_4^{-0.8} EM_{\perp \text{pc}} \text{ photons cm}^{-2} \text{ s}^{-1}, \quad (\text{A12})$$

where

$$\langle \epsilon_{\text{HA}}^* \rangle \equiv \int_{\nu_H}^{\infty} d\nu \frac{\langle \epsilon_{\nu A} \rangle}{h\nu} \quad (\text{A13})$$

is the ionizing photon luminosity per unit area of the galactic disk and the subscript “pc” on the emission measure indicates that it is measured in units of $\text{cm}^{-6} \text{ pc}$.

In the absence of extinction, the H α photon intensity in Rayleighs is

$$I^*(\text{H}\alpha) = \frac{\alpha_{\text{H}\alpha}}{4\pi} EM \left(\frac{1 \text{ R}}{10^6/4\pi \text{ photons}} \right) = 0.364 T_4^{-0.9} EM_{\text{pc}} \text{ R}, \quad (\text{A14})$$

where $\alpha_{\text{H}\alpha} \simeq 1.18 \times 10^{-13} T_4^{-0.9} \text{ cm}^3 \text{ s}^{-1}$ is the effective recombination coefficient for H α (from Osterbrock 1989). The relationship between the H α intensity normal to the disk and the surface emissivity (eq. A12) is almost independent of temperature,

$$I_{\perp}^*(\text{H}\alpha) = 4.55 \times 10^{-7} T_4^{-0.1} \langle \epsilon_{\text{HA}}^* \rangle \text{ R}. \quad (\text{A15})$$

These results can be readily extended to the recombination lines of helium, such as He I $\lambda 5876$. Ionization equilibrium in a column normal to the disk gives

$$\zeta_{\text{He}^0 A} = y_{\text{He}^0} \langle \epsilon_{\text{He}^0 A}^* \rangle \simeq \alpha_{\text{He}^0}^{(2)} \int dz n_e n(\text{He}^+), \quad (\text{A16})$$

where y_{He^0} is the fraction of the helium ionizing photons that are absorbed by neutral helium and $\alpha_{\text{He}^0}^{(2)} \simeq 2.73 \times 10^{-13} T_4^{-0.67} \text{ cm}^3 \text{ s}^{-1}$ is the recombination coefficient to excited states of He⁰ (from Osterbrock 1989). As written, the equation is approximate because, in contrast to hydrogen, not

all the recombinations to the ground state result in the ionization of another helium atom. The intensity of the λ 5876 line is

$$I(5876) = \frac{\alpha_{5876}}{4\pi} \int dz n_e n(\text{He}^+), \quad (\text{A17})$$

where $\alpha_{5876} \simeq 4.9 \times 10^{-14} T_4^{-1.1} \text{ cm}^3 \text{ s}^{-1}$ is the effective recombination coefficient for this line (from Osterbrock 1989). As a result, we find

$$I^*(5876) = 1.8 \times 10^{-7} y_{\text{He}^0} T_4^{-0.4} \langle \epsilon_{\text{He}^0 A}^* \rangle \text{ R}. \quad (\text{A18})$$

A.2. Opacity in a Cloudy Medium

The interstellar medium is highly inhomogeneous. In the simplest idealization, this inhomogeneity can be represented by clouds of opacity τ_c embedded in a transparent intercloud medium. The opacity in a cloudy medium was derived by Bowyer & Field (1969). If the expected number of clouds along the line of sight is \mathcal{N}_{los} , then the expected value of the ratio of the observed intensity I_ν to the emitted intensity $I_{\nu 0}$ is

$$I_\nu / I_{\nu 0} = \left(1 + \mathcal{N}_{\text{los}} e^{-\tau_{c\nu}} + \frac{1}{2!} \mathcal{N}_{\text{los}}^2 e^{-2\tau_{c\nu}} \dots \right) e^{-\mathcal{N}_{\text{los}}}, \quad (\text{A19})$$

$$= \exp[-\mathcal{N}_{\text{los}}(1 - e^{-\tau_{c\nu}})], \quad (\text{A20})$$

where the different terms in the series represent the contribution to the expected intensity if there are no clouds along the line of sight, one cloud, two clouds, etc. Thus, the expected value of the optical depth in a medium composed of identical clouds is

$$\tau_\nu = \mathcal{N}_{\text{los}} (1 - e^{-\tau_{c\nu}}). \quad (\text{A21})$$

In the limit of small $\tau_{c\nu}$, the expected optical depth reduces to $\mathcal{N}_{\text{los}} \tau_{c\nu}$, the value for a uniform medium. On the other hand, in the limit of large $\tau_{c\nu}$, the expected optical depth is \mathcal{N}_{los} , since the probability that a ray will not encounter any clouds is $\exp(-\mathcal{N}_{\text{los}})$.

If the total HI column density of the disk and halo is $N_{\text{H}^0 \perp}$ and that of an individual cloud is $N_{\text{H}^0 c}$, then

$$\tau_{0\nu} = \frac{N_{\text{H}^0 \perp}}{N_{\text{H}^0 c}} (1 - e^{-N_{\text{H}^0 c} \sigma_\nu}), \quad (\text{A22})$$

where σ_ν is the absorption cross section of the cloud material.

If the clouds are not all identical, the above argument is readily generalized (Bowyer & Field 1969). The expected opacity is

$$\kappa_\nu = \frac{d\tau_\nu}{ds} = \frac{d\mathcal{N}_{\text{los}}}{ds} (1 - e^{-\tau_{c\nu}}) \equiv \frac{1}{\lambda_c} (1 - e^{-\tau_{c\nu}}), \quad (\text{A23})$$

where ds is an element of distance along the line of sight and λ_c is the cloud mean free path. In terms of the area of a cloud, A_c , and the number of clouds per unit volume, $d\mathcal{N}/dV$, the mean free path is

$$\frac{1}{\lambda_c} = A_c \frac{d\mathcal{N}}{dV}. \quad (\text{A24})$$

If the clouds have a spectrum of masses, then the expected opacity becomes

$$\kappa_\nu = \int dM A_c(M) \frac{d^2\mathcal{N}}{dV dM} \left[1 - e^{-\tau_{c\nu}(M)} \right]. \quad (\text{A25})$$

Finally, we note that the specific intensity calculated with this value of κ_ν is approximately equal to that in the *intercloud* medium, provided the filling factor of the intercloud medium f_{ic} is close to unity. The solution of the equation of radiative transfer for a constant source function is

$$I_\nu = S_\nu (1 - e^{-\tau_\nu/\mu}). \quad (\text{A26})$$

If τ_ν or $\tau_{c\nu}$ is small, there is no distinction between the intensity in the clouds and that in the intercloud medium, so we focus on the case in which both optical depths are large. In that case,

$$I_\nu \simeq S_\nu = \frac{j_\nu}{\kappa_\nu} \simeq j_\nu \lambda_c. \quad (\text{A27})$$

In a cloudy medium, $j_\nu = j_{\nu,ic} f_{ic}$, where $j_{\nu,ic}$ is the emissivity in the intercloud medium. If the intercloud filling factor is close to unity, then $I_\nu \simeq j_{\nu,ic} \lambda_c$, which is the expected value of the intensity in the intercloud medium when τ_ν and $\tau_{c\nu}$ are large.

REFERENCES

- Arabadjis, J. S., & Bregman, J. N. 1999, ApJ, 510, 806
- Bakes, E. L. O. & Tielens, A. G. G. M. 1998, ApJ, 499, 258
- Baldwin, J. A., Ferland, G. J., Martin, P. G., Corbin, M. R., Cota, S. A., Peterson, B. M., & Slettebak, A. 1991, ApJ, 374, 580
- Birk, G. T., Lesch, H. & Neukirk, T. 1998, MNRAS, 296, 165
- Bowyer, S. & Field, G., 1969, Nature 223, 573
- Brickhouse, N. S. 1999, Astronomical Data Analysis Software and Systems VIII, ASP Conference Series, Vol. 172., eds. D. M. Mehringer, R. L. Plante, D. A. Roberts, (Provo:ASP)
- Cowie, L.L., & McKee, C.F. 1977, ApJ, 211, 135
- Cox, D. P., 1998 Proceedings of the IAU Colloquium No. 166 “The Local Bubble and Beyond”, eds. D. Breitschwerdt, M. J. Freyberg, J. Trümper, Lecture Notes in Physics 506, 121
- Cox, D. P. & Anderson, P. R. 1982, ApJ, 253, 268
- Cox, D. P. & McCammon, D. 1986, ApJ, 304, 657
- Cui, W., Sanders, W. T. & McCammon, D. 1996, ApJ, 468, 102
- Dickey, J.M., & Lockman, F.J. 1990, ARA&A, 28, 215
- Dove, J. B. & Shull, J. M. 1994, ApJ, 430, 222
- Edgar, R. J. 1986, ApJ, 308, 389
- Edgar, R. J. & Cox, D. P. 1993, ApJ, 413, 190
- Ferland, G. J. 1996, *Hazy, a Brief Introduction to Cloudy*, University of Kentucky Department of Physics and Astronomy Internal Report
- Garmire, G.P., Nousek, J.A., Apparao, K.M.V., Burrows, D.N., Fink, R.L., & Kraft, R.P. 1992, ApJ, 399, 694
- Hausen, N. R., Reynolds, R. J., Tufte, S. L. & Haffner, L. M. 1999, BAAS, 194, 47.19
- Haffner, L.M., Reynolds, R. J., & Tufte, S. L. 1999, ApJ, 523, 223
- Jakobsen, P. & Kahn, S. M. 1986, ApJ, 309, 682
- Jenkins, E. B., Jura, M. & Loewenstein, M. 1983, ApJ, 270, 88
- Kulkarni, S.R., & Fich, M. 1985, ApJ, 289, 792

- Maloney, P. R., Hollenbach, D. J. & Tielens, A. G. G. M. 1996, *ApJ*, 466, 561
- McCammon, D., Burrows, D. N., Sanders, W. T., & Kraushaar, W. L. 1983, *ApJ*, 269, 107
- McKee, C. F., 1998 Proceedings of the IAU Colloquium No. 166 “The Local Bubble and Beyond”, eds. D. Breitschwerdt, M. J. Freyberg, J. Trümper, *Lecture Notes in Physics* 506, 565
- McKee, C. F. & Cowie, L. L. 1977, *ApJ*, 215, 213
- McKee, C. F., & Ostriker, J. P. 1977, *ApJ*, 218, 148
- McKee, C.F. & Slavin, J.D. 1999 in *Interstellar Turbulence, Proceedings of the 2nd Guillermo Haro Conference*, eds. Franco, J & Carramiñana, A, (city: Cambridge Univ. Press)
- McKee, C.F. & Williams, J.P. 1997, *ApJ*, 476, 144
- Miller, W. W. 1994, Ph.D. thesis, University of Wisconsin-Madison
- Miller, W. W. & Cox, D. P. 1993, *ApJ*, 417, 579
- Minter, A. & Balser, D. S. 1998 Proceedings of the IAU Colloquium No. 166 “The Local Bubble and Beyond”, eds. D. Breitschwerdt, M. J. Freyberg, J. Trümper, *Lecture Notes in Physics* 506, 543
- Osterbrock, D. E., 1989, *Astrophysics of Gaseous Nebulae and Active Galactic Nuclei* (Mill Valley, CA: University Science Books)
- Pifer, R.J., Tufte, S.L., Reynolds, R.J., & Haffner, L.M. 1999, *BAAS*, 31, 891
- Raymond, J. C. & Smith, B. W. 1977, *ApJS*, 35, 419
- Raymond, J. C. 1992, *ApJ*, 384, 502
- Reynolds, R. J. 1984, *ApJ*, 282, 191
- Reynolds, R. J. 1985a, *ApJ*, 294, 256
- Reynolds, R. J. 1985b, *ApJ*, 298, L27
- Reynolds, R. J. 1988, *ApJ*, 333, 341
- Reynolds, R. J. 1989a, *ApJ*, 339, L29
- Reynolds, R. J. 1989b, *ApJ*, 345, 811
- Reynolds, R. J. 1990, *ApJ*, 348, 153
- Reynolds, R. J. 1991, *ApJ*, 372, L17
- Reynolds, R. J. & Cox, D. P. 1992, *ApJ*, 400, L33

- Reynolds, R. J., Haffner, L. M., & Tufte, S. L. 1995, *ApJ*, 525, L21
- Reynolds, R. J. & Tufte, S. L. 1995, *ApJ*, 439, L17
- Reynolds, R. J., Tufte, S. L., Haffner, L. M., Jaehner, K. & Percival, J. W. 1998, *Publ. Astron. Soc. Aust.*, 15, 14
- Savage, B. D., Sembach, K. R. & Lu, L. 1997, *AJ*, 113, 2158
- Sciama, D. W. 1990, *ApJ*, 364, 549
- Sciama, D. W. 1995, *ApJ*, 448, 667
- Sciama, D. W. 1997, *ApJ*, 488, 234
- Shull, J. M. & Slavin, J. D. 1994, *ApJ*, 427, 784
- Slavin, J. D., 1998 *Proceedings of the IAU Colloquium No. 166 “The Local Bubble and Beyond”*, eds. D. Breitschwerdt, M. J. Freyberg, J. Trümper, *Lecture Notes in Physics* 506, 169
- Slavin, J. D. & Cox, D. P. 1992, *ApJ*, 392, 131
- Slavin, J. D. & Cox, D. P. 1993, *ApJ*, 417, 187
- Slavin, J. D., Shull, J. M. & Begelman, M. C. 1993, *ApJ*, 407, 83
- Smith, R. K. & Cox, D. P. 1998, *Proceedings of the IAU Colloquium No. 166 “The Local Bubble and Beyond”*, eds. D. Breitschwerdt, M. J. Freyberg, J. Trümper, *Lecture Notes in Physics* 506, 133
- Snowden, S. L., Freyberg, M. J., Plucinsky, P. P., Schmitt, J. H. M. M., Trümper, J., Voges, W., Edgar, R. J., McCammon, D. & Sanders, W. T. 1995, *ApJ*, 454, 643
- Snowden, S. L., Egger, R., Freyberg, M. J., McCammon, D., Plucinsky, P. P., Sanders, W. T., Schmitt, J. H. M. M., Trümper, J. & Voges, W., 1997, *ApJ*, 485, 125
- Snowden, S. L., Egger, R., Finkbeiner, D. P., Freyberg, M. J. & Plucinsky, *ApJ*, 493, 715
- Spitzer, L. & Fitzpatrick, E. 1993, *ApJ*, 409, 299
- Vacca, W. D., Garmany, C. D. & Shull, J. M. 1996, *ApJ*, 460, 914
- Vallerga, J. V. & Slavin, J. D. 1998 *Proceedings of the IAU Colloquium No. 166 “The Local Bubble and Beyond”*, eds. D. Breitschwerdt, M. J. Freyberg, J. Trümper, *Lecture Notes in Physics* 506, 79
- Wolfire, M. G., Hollenbach, D., McKee, C. F., Tielens, A. G. G. M. & Bakes, E. L. O. 1995, *ApJ*, 443, 152

Wolfire, M. G., McKee, C. F., Hollenbach, D., & Tielens, A. G. G. M. 1995, ApJ, 453, 673

Wolfire, M. G., McKee, C. F., Hollenbach, D., & Tielens, A. G. G. M. 2000, ApJ, 000, 000

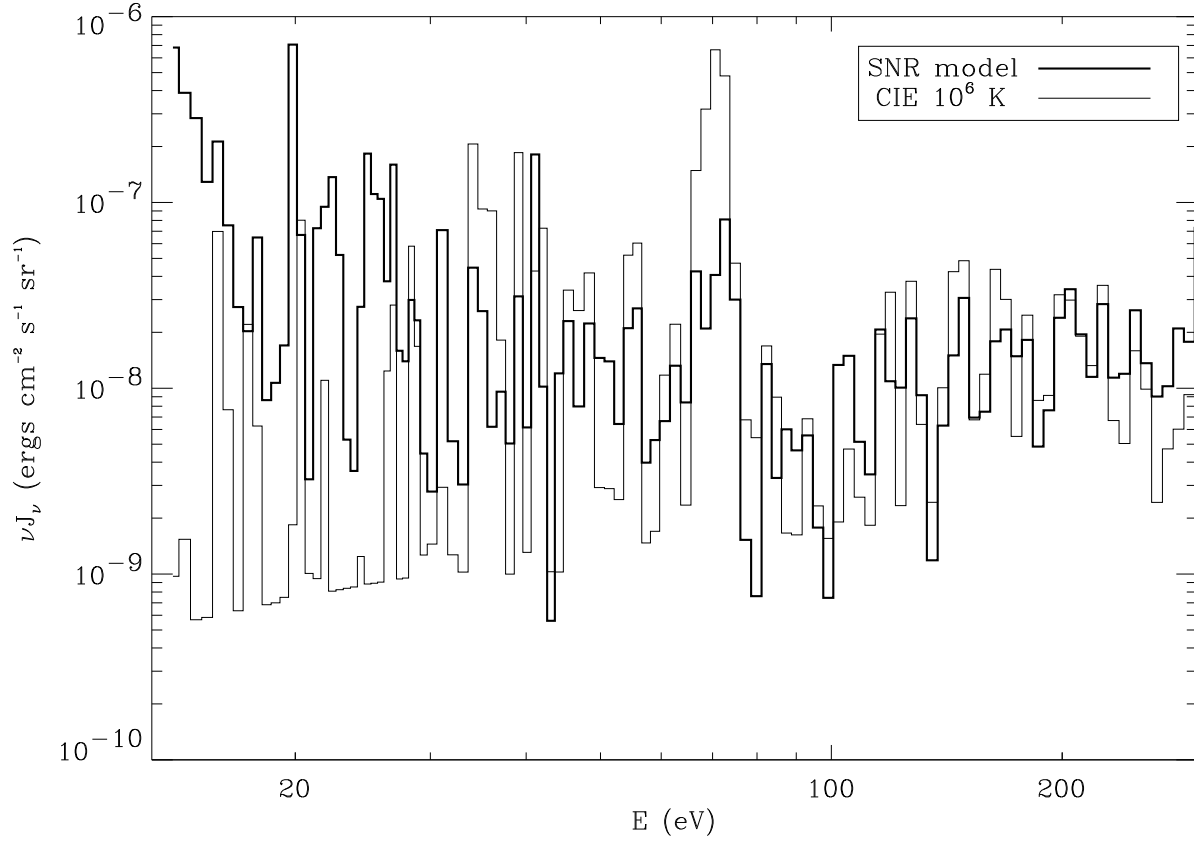


Fig. 1.— Mean intensity incident on a typical cloud for our model spectrum with ambient density 0.1 cm^{-3} and no conductivity. For comparison we also plot the mean intensity of a collisional ionization equilibrium, $T = 10^6 \text{ K}$ plasma with the emission chosen to match the all-sky average for the Wisconsin B band observations. (The CIE spectrum does not provide quite enough emission to match the all-sky average C band rate.)

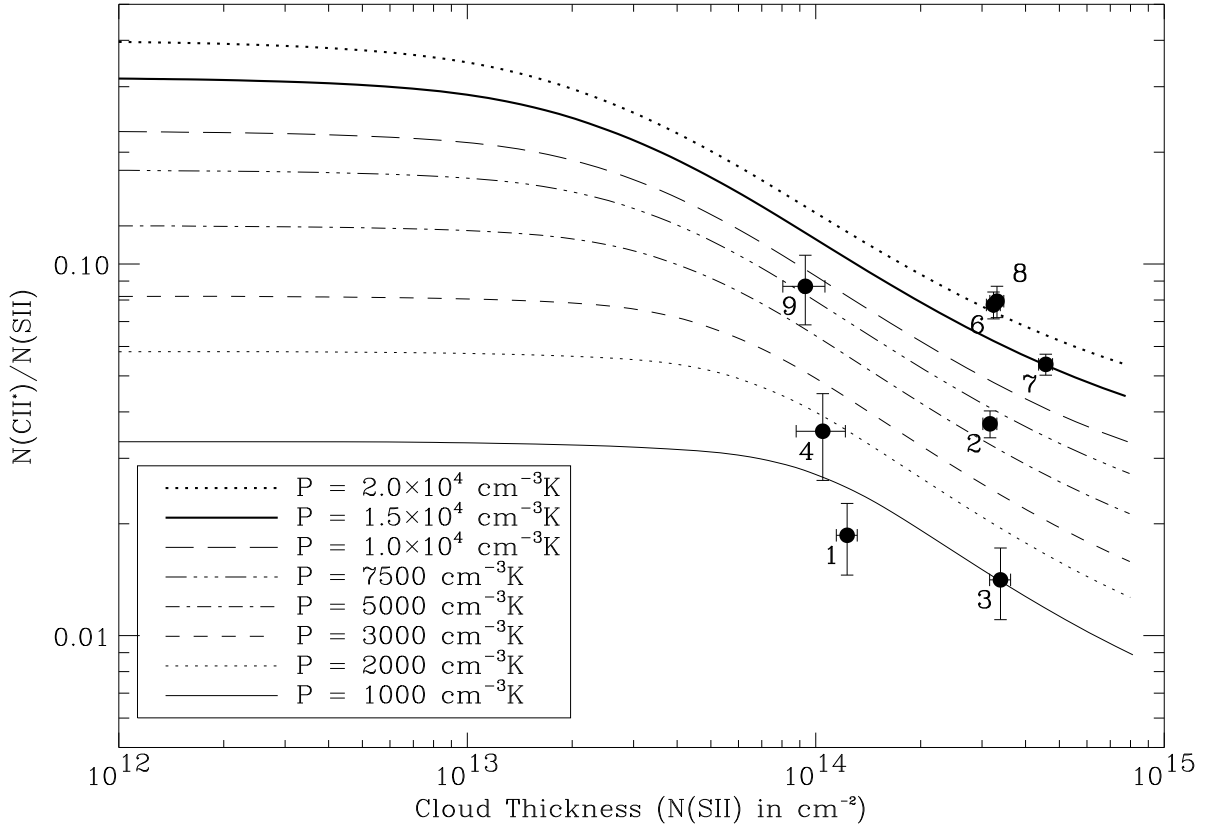


Fig. 2.— Ionization created by our model spectrum incident upon clouds at different thermal pressures vs. thickness of the cloud. It is clear that slow clouds in particular (nos. 6–9) demand high pressures to be consistent with both the $H\alpha$ and absorption line observations.

Table 1. Spectral Characteristics of SNR Spectra

n_a (cm^{-3})	thermal conduction	ϕ_{H}	ϕ_{He^0}	ϕ_{He^+}	ϕ_X	$Q(\text{He}^0)/Q(\text{H}^0)$
0.04	n	0.32	0.096	0.038	0.0015	0.15
0.04	y	0.31	0.091	0.039	0.0018	0.15
0.1 ^a	n	0.39	0.11	0.052	0.0032	0.15
0.1	y	0.38	0.12	0.054	0.0036	0.16
0.3	n	0.42	0.14	0.076	0.0053	0.17
0.3	y	0.42	0.13	0.077	0.0052	0.17
1.0	n	0.39	0.16	0.10	0.0077	0.20
1.0	y	0.36	0.14	0.10	0.0080	0.20

^aStandard model

Table 2. Photoionization Due to SNR Emission

n_a (cm^{-3})	thermal conduction	$(EM_{\perp\text{pc}}/2)^a$ ($\text{cm}^{-6} \text{pc}$)	$h\bar{\nu}_H$ (eV)	$\mathcal{N}_\gamma(> \nu_H)$ (10^{61} photons)	$\phi(> \nu_H)$
0.04	n	0.93	19.9	1.4	0.45
0.04	y	0.92	19.9	1.4	0.45
0.1	n	1.2	19.5	1.8	0.56
0.1	y	1.2	19.8	1.8	0.56
0.3	n	1.3	20.2	2.0	0.64
0.3	y	1.3	20.1	2.0	0.64
1.0	n	1.2	22.0	1.9	0.66
1.0	y	1.2	21.4	1.8	0.62

^aEmission measure for the half disk; assumes $T = 8000$ K

Table 3. Comparison of Data with Model Results

	Slow		Fast	
	Observed	Model ^a	Observed	Model ^a
$N(\text{S II})/(10^{14} \text{ cm}^{-2})$	12	12	8.8	8.8
$N(\text{C II}^*)/(10^{13} \text{ cm}^{-2})$	8.4	8.1 – 8.5	2.3	2.5 – 2.3
$I(\text{H}\alpha) (R)$	0.22	0.19	0.16	0.19
$N(\text{H I})/(10^{19} \text{ cm}^{-2})$	6.8	7.6 – 7.6	4.9	4.7 – 4.3
$N_e/(10^{18} \text{ cm}^{-2})$...	4.9 – 5.5	...	16 – 21
$N(\text{S III})/N(\text{S II})$...	0.050 – 0.051	0.10	0.087 – 0.10
$I(5876) (R)$...	0.0048 – 0.0044	...	0.0053 – 0.0051
$I(6300) (R)$...	0.16 – 0.53	...	0.044 – 0.12
$I(6716) (R)$	0.24	0.38 – 0.92	0.19	0.14 – 0.30
$I(6584) (R)$	0.22	0.058 – 0.20	0.29	0.064 – 0.19
$\langle P \rangle/(1000 \text{ cm}^{-3}\text{K})$...	10 – 15	...	1.5 – 1.8
$N(\text{H I})_{X\text{-ray}}/N(\text{H I})$...	1.028 – 1.032	...	1.172 – 1.251

^aThe range of results is for models with $T = 6000 - 8000$ K; see text.